Soils and Foundations 2013;53(2):299–314

The Japanese Geotechnical Society

Soils and Foundations

www.sciencedirect.com
journal homepage: www.elsevier.com/locate/sandf

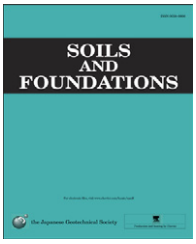

Mechanical and dissociation properties of methane hydrate-bearing sand in deep seabed

Masayuki Hyodo[a], Jun Yoneda[b,*], Norimasa Yoshimoto[a], Yukio Nakata[a]

[a]*Graduate School of Science and Engineering, Yamaguchi University, Japan*
[b]*The National Institute of Advanced Industrial Science and Technology (AIST), Japan*

Received 13 June 2011; received in revised form 5 January 2012; accepted 19 January 2013
Available online 9 March 2013

Abstract

A series of triaxial tests has been carried out on the mechanical properties and dissociation characteristics of sands containing methane hydrate using an innovative high pressure apparatus which has been developed to reproduce the in-situ conditions expected during proposed methane extraction methods. It was found that the strength of MH sand increased with MH saturation due to particle bonding. Dissociation by heating caused large axial strains for samples with an initial shear stress and total collapse for samples consolidated in the metastable zone. In the case of dissociation by de-pressurization, axial strains were generated by increasing effective stress until a stable equilibrium was reached. However, re-pressurization led to the collapse in the metastable zone.
© 2013 The Japanese Geotechnical Society. Production and hosting by Elsevier B.V. All rights reserved.

Keywords: Methane hydrate-bearing sand; Triaxial compression test; High pressure; Temperature; Back pressure; Strength; Stiffness; Stability; (IGC: B10/D6)

1. Introduction

Methane hydrate (MH) is a solid compound in which a large amount of methane is trapped within a crystalline structure of water, forming a solid similar to ice. It is known to exist in a stable condition under certain temperature and pressure conditions. Its existence has been confirmed in permafrost layers and in deep ocean floors (Kvenvolden et al., 1993). Although Japan has no permafrost zones, it is believed that MH exists in the seafloor, and development is underway for MH to be a future energy resource, replacing oil and coal (MH21 Research Consortium, 2001; Nagakubo, 2009). Recently, the existence of a large-scale MH natural gas reservoir has been investigated in the Nankai Trough (Fujii et al., 2008, 2009). Worldwide, MH is believed to exist in various forms, such as massive structures within muddy layers or at the surface of deep seabeds, or embedded within the pores of sandy layers (Waite et al., 2009). The seabed in the Nankai Trough consists of alternating layers of sand and clay, and it has been confirmed that the MH-enriched zone is buried within the voids of the sand layer (Suzuki et al., 2009).

Currently, the method proposed for abstracting methane in the Nankai Trough is by drilling a shaft into the MH-rich layer, and heating, depressurizing, or inserting hydrate inhibitors, causing the MH to become dissociated into methane and water after which the gas could be collected (Yamamoto, 2009). Using these methods, the solid MH existing in the pores within the soil is transformed into gas for collection; in the process, complex physical events, such

*Corresponding author. Tel.: +81 29 861 8306; fax: +81 29 861 8765.
E-mail address: jun.yoneda@aist.go.jp (J. Yoneda).
Peer review under responsibility of The Japanese Geotechnical Society.

0038-0806 © 2013 The Japanese Geotechnical Society. Production and hosting by Elsevier B.V. All rights reserved.
http://dx.doi.org/10.1016/j.sandf.2013.02.010

as changes in the soil structure and thermal conductivity, pore fluid and gas migration, and other complicated phenomena need to be considered. It is predicted that a combination of such phenomena could cause consolidation and shear deformation of the ground due to changes in the effective stress and decrease in soil particle strength. Therefore, it is important to investigate the mechanical properties of MH-bearing sediments, for safe and economical exploitation.

Based on the author's experience of triaxial testing of sand specimens (Yasufuku et al., 1991; Hyodo et al., 2002), the investigation of the mechanical behavior of MH-bearing sediments was started using a triaxial compression test apparatus equipped with a high-pressure cell inside a freezer. Isotropic consolidated undrained triaxial compression tests were performed on specimens consisting of granulated MH and sand prepared by mixing and compacting mixture of MH powder and sand to investigate the effects of temperature and confining pressure on the strength characteristics of MH and sand mixtures (Hyodo et al., 2002, 2005). As a result, it was found that the shear strength of MH sand mixture increased with MH content increase. In addition, the shear strength of MH sand mixtures was found to increase with decrease in temperature and increase in confining pressure. The development of a testing apparatus which could more accurately reproduce the deep seabed temperature and stress conditions was initiated and a triaxial compression test machine was developed that could simulate predicted temperature changes in-situ and during the MH production process and apply high back (pore water) pressure and confining pressure corresponding to those existing in-situ. The dissociation of MH by heating and de-pressurization could be reproduced and the investigation of the deformation response of MH-bearing sands during the MH dissociation process became possible (Hyodo et al., 2007, 2008; Yoneda et al., 2007a, 2007b). Using this apparatus, methane gas could be injected into moist sand within the cell to produce MH dispersed around the soil particles similar to that occurring in deep seabed conditions. The authors performed consolidated drained triaxial compression tests on MH-bearing sediments under a similar physical environment to that found in-situ and an empirical equation for predicting strength of MH-bearing sediments associated with temperature, water pressure and MH saturation has been proposed (Yoneda et al., 2007a, 2007b). K_0 consolidated drained triaxial compression tests were also performed on undisturbed sediments from the Nankai Trough. These showed the mechanical properties of undisturbed sediments and artificially prepared sediments to be quite similar (Yoneda et al., 2010).

Miyazaki et al. (2007) performed triaxial compression tests with varying strain rates to investigate the shear strength characteristics and shear rate dependency for medium and large-strain ranges. They performed triaxial compression tests on dense specimens with varying confining pressures, and an empirical equation for predicting shear strength of MH-bearing sediments related to confining pressure was proposed. In addition, employing a comparatively low pressure to generate hydrate from THF (tetrahydratefuran), Yun et al. (2007) formed hydrate within sand, silt and kaolinite using THF-saturated water and carried out compression tests on hydrate-bearing sand with 0% to 100% of hydrate saturation. The results indicated that the increase in shear strength was small for THF-hydrate saturation ratios less than 40% but a marked increase in shear strength was observed when the saturation ratios exceeded 40%.

For the consideration of deformation due to MH production, a one-dimensional cylinder type experiment is commonly used. Sakamoto et al. (2008) used the de-pressurization method to dissociate the hydrate in MH-bearing sand and based on the observed one-dimensional compression behavior, they examined the changes in the seepage characteristics. Lee et al. (2010) also investigated settlement by hydrate formation and dissociation within sand, silt and kaolinite using THF under various confining pressures. These results are valuable for predicting settlement simply due to de-pressurization. However, in the case of there being some initial shear stress, the deformation caused by de-pressurization with dissociation of MH is still not clear.

A series of triaxial tests has been carried out in this study in order to investigate the mechanical properties and dissociation characteristics of methane hydrate bearing sand using an innovative high pressure apparatus which has been developed to reproduce the in-situ conditions.

2. Testing equipment and sample preparation

2.1. Triaxial testing apparatus

To reproduce the stress and temperature conditions in the deep seabed and to examine the mechanical behavior of MH-bearing sand specimens under such conditions and when MH is produced, a temperature-controlled high pressure triaxial testing apparatus was developed where the pore pressure and confining pressure could be controlled under various temperature and high pressure conditions. Fig. 1(a) shows the physical appearance of the device, while Fig. 1(b) shows a schematic diagram of the testing system. A detailed description of each part shown in Figure is presented below.

(a) *Test specimen*

A cylindrical frozen specimen measuring 30 mm in diameter × 50 mm high, or 50 mm in diameter × 100 mm high was used.

(b) *Pedestal*

To prevent the dissociation of natural MH samples, test specimens had to be set-up rapidly. For this purpose, the pedestal in the present apparatus was

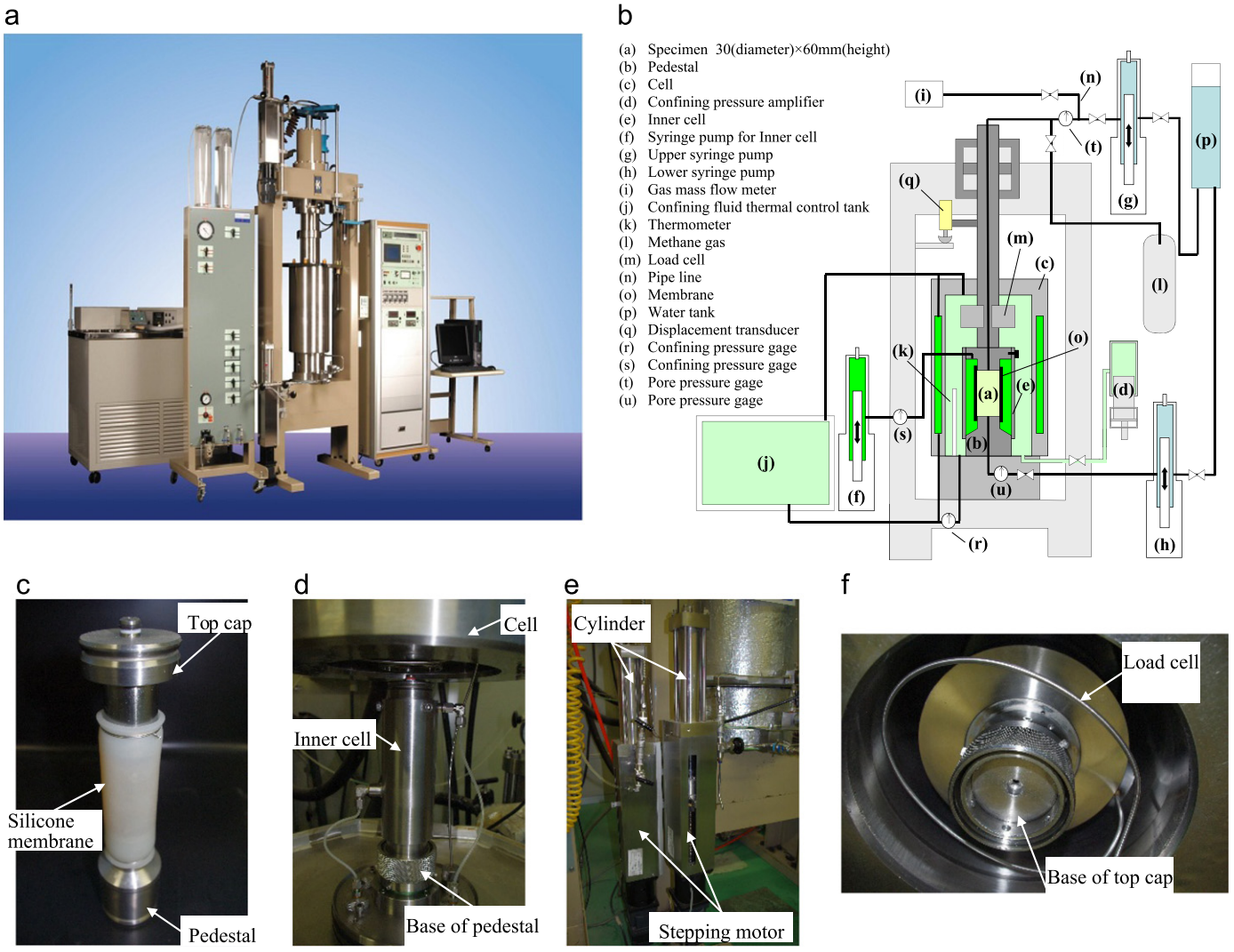

Fig. 1. Experimental apparatus. (a) Exterior view of the temperature-controlled high pressure triaxial device, (b) cell appurtenances and piping system, (c) set up frozen sand specimen, (d) set up of Inner cell, (e) Syringe pump and (f) load cell and base of top cap.

designed to be a one-touch removable socket-type, as shown in Fig. 1(c).

(c) *Cell*

The cell was designed to resist a pressure of 30 MPa, with a mechanism that allowed cell fluid to circulate internally to control the temperature.

(d) *Cell pressure generation device*

Cell pressures of up to 30 MPa controllable within the range of ± 0.1 MPa were supplied by oil pressure.

(e) *Inner cell*

Because of the possibility for the specimen to become unsaturated during a test, a double cell was adopted to measure the volume change. The change in volume could be obtained by measuring the water level difference in the cell while the upper part was opened; however, since high pressures were used, with penetration of the piston in the sealed-up cylinder controlling the pressure, making it possible to measure the volume change, as shown in Fig. 1(d).

(f) *Syringe pump for inner cell*

To measure the volume change in the inner cell, a cylinder designed to resist pressures up to 30 MPa was installed and the change in volume inside the cylinder was measured by controlling the piston in the cylinder via a pulse-controlled method using a stepping motor. In addition, the change in volume of unsaturated specimens was measured by correcting the amount of piston penetration, as shown in Fig. 1(e).

(g) *Upper syringe pump*

High pressure triaxial compression test equipment used in geotechnical engineering up to now has been made to reproduce the ground stress under high confining pressure. However, the pore water pressure associated with the high pressure condition needed to reproduce the large depths where MH could exist has not previously been considered. For this device, a mechanism similar to the syringe pump for the inner cell (f) was installed, adding this function to the

apparatus. At the extreme condition of 20 MPa, it was possible to control the pressure to within ± 0.05 MPa. Moreover, by using an incompressible solution in the cylinder, the measurement of the volume change of the specimen was enabled by calculating the amount of penetration of the piston in the cylinder from the pulse. The pipe was made of stainless steel so that it could withstand high pressure. This was the main feature of this testing apparatus and, as a result, the high pore pressure in the deep seabed could be reproduced.

(h) *Lower syringe pump*

A mechanism similar to (g) was also installed.

(i) *Gas mass flow meter*

To calculate the MH saturation ratio, a mass flow meter for the gas was installed in the pipe. The gas that passed the device was measured as mass flow (in g/min) independent of temperature and pressure, and shown as flow volume (in mL/min) standardized at 20 °C and −1 atm. In addition, the amount of gas could be measured by calculation. The measurement range was 0–500 mL/min, and when MH was dissociated after the end of shearing, the amount of gas was measured while adjusting the valve in the pipe equipped with the mass flow meter and connected to the specimen.

(j) *Device controlling the liquid temperature*

This device consisted of a system to adjust the temperature from −35 °C to +50 °C within the triaxial cell by circulating the cell fluid in the triaxial testing device from an external temperature controlled water tank. The temperature in the tank could be controlled within a range of ±0.1 °C. To conduct tests at low temperature, it was possible to use a fluid with a freezing point below −40 °C or to use aurorabrine, which has excellent corrosion performance when in contact with various metallic materials.

(k) *Thermometer*

A thermometer was installed near the side of the specimen in the triaxial room, and the temperature in the triaxial room could be measured. The temperature in the cell was controlled based on the value indicated by the thermometer. When the temperature was changed while performing the tests, adequate time was provided until the temperature of the fluid and the specimen equalized.

(l) *Methane gas cylinder*

Methane for producing methane hydrate was stored in a gas cylinder which for safety reasons was installed outdoors.

(m) *Load cell*

To eliminate the influence of piston friction, a cylindrical-shaped loading cell that could not be affected by temperature and pressure was set up in the cell. The maximum permissible load was 200 kN, and it was possible to measure with accuracy of up to 1/1000 of the full scale load, as shown in Fig. 1(f).

(n) *Pipe*

Methane gas flowed inside the pipe after the test and to prevent the accumulation of gas, the pipe was oriented vertically and as short a pipe as possible was used.

(o) *Membrane*

Because the specimens in the tests were subjected to low temperatures and high pressures, latex membranes conventionally used in triaxial tests were avoided; instead, silicon-type membranes were used because of their flexibility under low temperature and high pressure conditions. Note that because methane gas can permeate through silicon to some degree, butyl rubber was used in long term tests, such as during MH dissociation.

The measuring apparatus was connected to a data collection system, with the vertical load, axial displacement, confining pressure, volume change of specimen and pore water pressure automatically recorded by a personal computer. To verify the accuracy of the measuring devices, the following shear tests were done using samples of silica sand without MH.

2.2. Specimen preparation

Based on visual observation of the undisturbed core samples obtained from the Nankai Trough (Suzuki et al., 2006b), it is believed that MH in-situ is buried within the pores between grains of the sand. Based on this, MH-bearing sand was artificially produced using the grain size distribution curve of the undisturbed core sample (Suzuki et al., 2009) as shown in Fig. 2, and Toyoura sand was chosen as the host material. First, the amount of water for the target MH saturation was mixed with sand whose volume corresponded to a target density. The moist soil was placed in 15 layers in a mold measuring 30 mm in

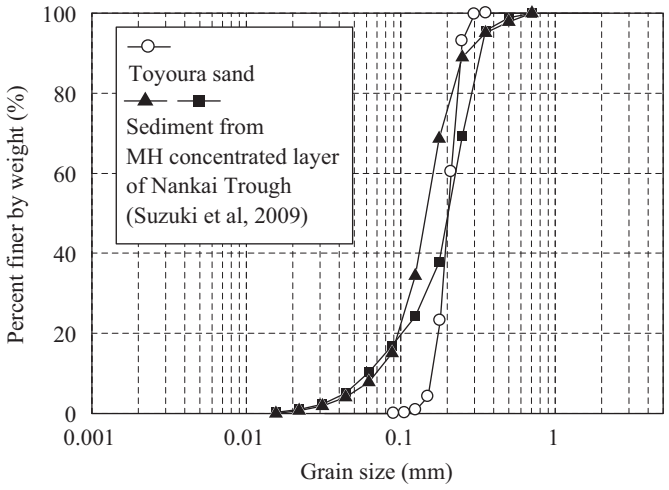

Fig. 2. Grain size distribution curves for Toyoura sand and sediments obtained from the Nankai Trough.

diameter and 60 mm high, with each layer compacted by a tamper 40 times. In order for the specimen to stand by itself, the mold containing the sand was placed in a freezer. The frozen specimen was then removed from the mold and placed on the pedestal, and the membrane was installed as shown in Fig. 1(c). Because the specimens in the tests were subjected to low temperature and high pressure, rubber membranes conventionally used in triaxial tests were avoided; instead, silicon-type membranes were used because of their flexibility under low temperature/high pressure conditions and butyl rubber was used in long term tests, such as MH dissociation because silicone is to some degree permeable to methane gas. The inner cell set up is shown in Fig. 1(d).

2.3. Generation of MH and experimental procedure

After forming the specimen, it was subjected to a series of processes under specific temperatures and pressures, as depicted in Fig. 3. First of all, the frozen specimen (a) was thawed to room temperature inside the triaxial cell (b). Then, the back pressure was gradually increased to 4 MPa while methane was injected into the specimen (c) by filling the pores of the specimen with methane. At this time, the gas pressure was increased over a period of time so that the specimen's moisture content would not become non-uniform as a result of the pressurized injection. Next, the temperature in the triaxial cell was lowered to 1 °C where the MH was stable, and the specimen environment was kept under constant temperature and pressure conditions for 24 h. By keeping the gas pressure constant in the connection between the specimen and the syringe pump and by observing the amount of gas flowing at various times, the transformation of water within the pores into hydrate was judged to be complete if there was no marked change in the amount of gas, as indicated in the Fig. 4.

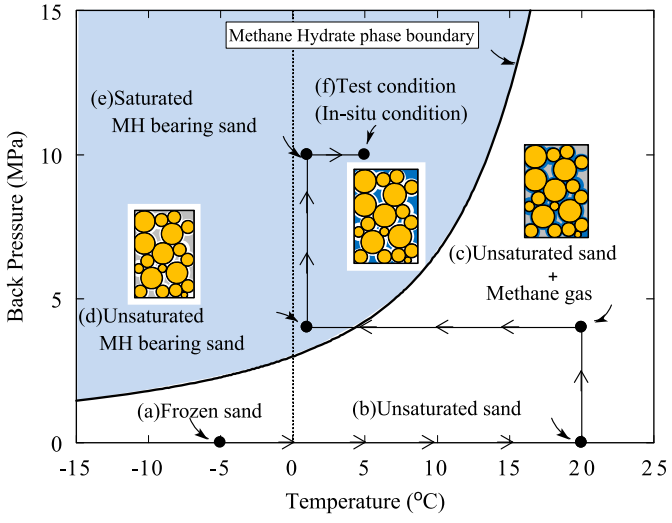

Fig. 3. State paths for pressure and temperature to produce MH-bearing sand.

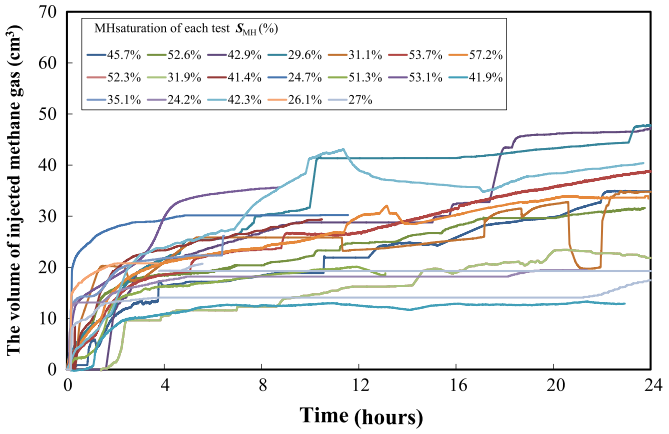

Fig. 4. Time histories of volume of methane gas injected into the MH-bearing sands.

Note that the plots in the figure show some irregularities because in inducing the gas to flow into the specimen to promote the generation of MH, the volume of gas in the specimen was increased and decreased slightly while adjusting the upper and lower syringe pumps.

After the hydrate was generated, pure water under constant pressure was allowed to infiltrate the specimen. The water infiltrated was not methane saturated. Although some dissociation of MH was anticipated by injecting pure water, new formation of MH may also occur by circulating the MH saturated water into the specimen. As we wish to specify the initial degree of MH saturation, we used pure water in the study. The degree of MH saturation was measured after the test by collecting the dissociated methane gas. As a result the exact degree of MH saturation which was almost same as the expected one was measured. Then, the back pressure was applied (e) and the temperature was adjusted to the prescribed test condition (f). While keeping the pressure constant, consolidation was carried out until the specified effective stress was reached and shearing was conducted with a strain rate of 0.1%/min.

When MH was to be generated after consolidation, the frozen specimen set up in the triaxial cell room was thawed immediately and consolidation was performed until the prescribed stress was reached. Then, methane gas was injected into the specimen and when the hydrate was generated in the MH stable zone, the sample was sheared at the same temperature and back pressure as MH was to be generated before consolidation. These cases were considered to examine the difference between the response of MH being generated in existing sedimentary soil layers and the case where soil layers sediment after MH was generated.

After shearing, the temperature in the specimen was increased and MH dissociated; the amount of gas was measured using the gas mass flow meter shown in Fig. 1(b). The amount of gas measured was then converted into MH saturation, assuming the density of MH was 0.913 mg/m^3 (Sloan, 1998).

Table 1
Test conditions and experimental results for triaxial compression tests.

Testing conditions			Testing results			
Effective confining pressure σ'_c(MPa)	Pore pressure $P.P$ (MPa)	Temperature T (°C)	Porosity n (%)	Degree of saturation by MH S_{MH} (%)	Deviator stress q_{max} (MPa)	Secant modulus E_{50} (MPa)
1	5	5	45.6	0	2.35	117
			45.0	45.7	2.69	270
	10	5	39.3	0	3.25	369
			39.4	54.3	4.20	497
			45.6	0	2.36	118
			45.3	45.0	2.76	329
3	5	5	39.4	0	7.02	501
			45.3	0	6.35	159
			39.6	42.9	7.45	483
			39.5	29.6	8.42	979
			45.3	31.1	6.69	322
			45.3	28.7	6.49	391
	10	5	39.2	0.0	7.28	321
			39.4	53.7	7.63	763
			39.3	38.7	7.90	841
			38.9	26.3	4.47	624
			45.4	69.5	7.00	510
			45.7	57.2	6.89	434
			45.3	50.4	6.54	399
	15	1	39.2	52.3	8.69	943
			39.6	31.9	7.76	690
			45.5	60.9	7.26	459
			45.2	43.7	6.61	397
		10	39.5	51.6	7.57	603
			45.4	48.3	6.69	485
5	10	1	39.4	41.4	13.55	782
			39.3	24.7	10.95	730
		5	39.4	0	10.32	653
			39.4	51.3	13.88	1068
			40.1	53.1[a]	14.74	1074
			39.1	41.9[a]	12.86	999
			39.2	35.1	11.84	761
			39.6	24.2	10.71	756
		10	39.2	42.3	12.18	693
			38.6	26.1	10.88	668
	15	5	39.0	27.0	10.88	887

[a]MH was formated after consolidation.

3. Triaxial compression tests

3.1. Testing condition

The experimental conditions equivalent to in-situ conditions and the corresponding experimental results are summarized in Table 1 for isotropically consolidated shear tests. In the experiments, the specimens were subjected to different levels of effective confining pressure (1, 3, 5 MPa), back pressure (5, 10, 15 MPa) and temperature (1, 5, 10 °C). For all tests, a shearing rate of 0.1%/min was adopted. Tests were performed on two sets of specimens, porosity $n=40\%$ (relative density $Dr=90\%$) and $n=45\%$ ($Dr=40\%$), with various MH saturation ratios. The maximum deviator stress indicated in the table refers to the peak stress obtained from the deviator stress–axial strain relation; however, if peak was not observed, the deviator stress corresponding to 15% axial strain was used.

3.2. Testing results

Fig. 5 shows the deviator stress, axial strain and volumetric strain relations for isotropically consolidated $n=40\%$ specimen ($Dr=90\%$) with different MH saturation and subjected to effective confining pressure $\sigma'_c=5$ MPa. From the figure, it is observed that the specimens show compressive volume change and strain hardening behavior at this level of confining pressure, notwithstanding the high relative density. Moreover, a marked increase in the initial stiffness and strength is observed as the MH saturation of MH-bearing specimen increases. The volumetric strain changed from compressive to dilative, and for

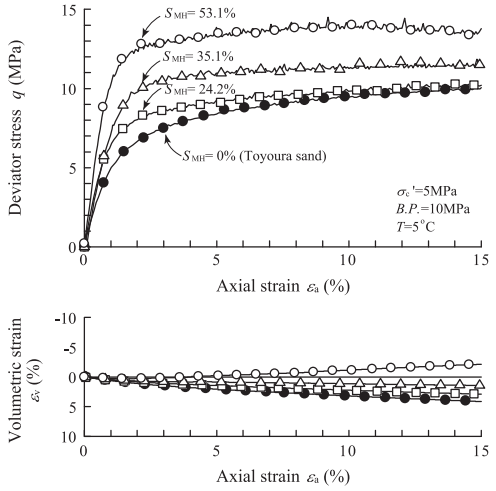

Fig. 5. Effects of MH saturation ratio on the shear behavior of isotropically consolidated MH-bearing sand.

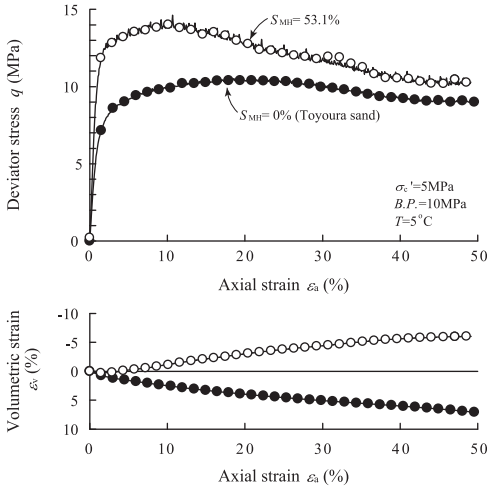

Fig. 6. Effect of effective confining pressure on the deviator stress, axial strain and volumetric strain relations for MH-bearing sand.

specimens with $S_{MH}=50\%$, significant dilative behavior was observed. This is believed to be due to the hardening action induced by MH on the sand particles. To explain this hardening action, reference is made to previous research conducted on the hardened soil structure of sand to which cement was added (Oda et al., 1998). Based on observation of the internal structure of the specimen with 4% and 7% cement, the authors postulated that when peak strength was mobilized, a mass of particle with strength corresponding to the hardened strength was generated at the shear surface; consequently at the residual state, a mass of the same strength as the particle was destroyed. Thus, they reported that the residual strength of the cemented sand was the same as the uncemented specimen. For the present test on MH-bearing sand with $S_{MH}<30\%$, a similar phenomenon can be assumed to occur. On the other hand, the higher residual strength observed in specimens with high S_{MH} is postulated to be due the contribution of MH flakes which were peeled off from sand particle surfaces and were buried within the pores of the sand during shearing, resulting in increased residual strength and increased positive-dilatancy.

Although axial strain $\varepsilon_a=15\%$ was exceeded in most tests, high residual strengths were observed in all cases, as shown in Fig. 5. In order to examine what extent of axial strain would affect the residual strength, tests were performed on a pure sand specimen and one with the highest MH saturation ($S_{MH}=53.1\%$) for axial strains up to $\varepsilon_a=50\%$, and the results are shown in Fig. 6. From the figure, the peak strength for the MH-bearing sand took place near $\varepsilon_a=12\%$ after which strain hardening started to occur at $\varepsilon_a=15\%$ and, although not shown in the figure, the deviator stress and volumetric strain remained constant up to about $\varepsilon_a=42\%$, indicating steady state conditions. On the other hand, although the pure sand specimen demonstrated a similar steady state condition, significant difference in residual strength can be observed even at $\varepsilon_a=50\%$. Next, the effect of the different MH generation

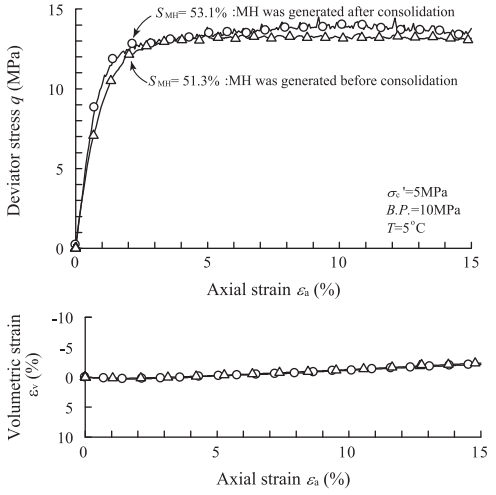

Fig. 7. Effect of MH generation process on the deviator stress, axial strain and volumetric strain relations of MH-bearing sand.

processes within the specimens was examined. For this purpose, the test results are compared for two cases: (1) a specimen where MH was produced at an effective confining pressure $\sigma'_c=0.2$ MPa after which it was consolidated at $\sigma'_c=5$ MPa; and (2) a specimen where MH was generated after the effective confining pressure $\sigma'_c=5$ MPa was applied. These cases were considered to investigate the effect of period for MH formation. The results of this comparative study are shown in Fig. 7 for $S_{MH}=50\%$. It is seen that the behavior of specimens in both cases are similar, indicating that the difference in MH generation process as discussed above does not have a significant effect on the shear response of the specimen.

Tests under different effective confining pressures ($\sigma'_c=1$ MPa, 3 MPa, 5 MPa) but with constant back pressure, temperature and MH saturation were performed to examine the influence of the effective confining pressure on the shear behavior of MH-bearing specimens. The test results for each confining pressure are shown in Fig. 8 together

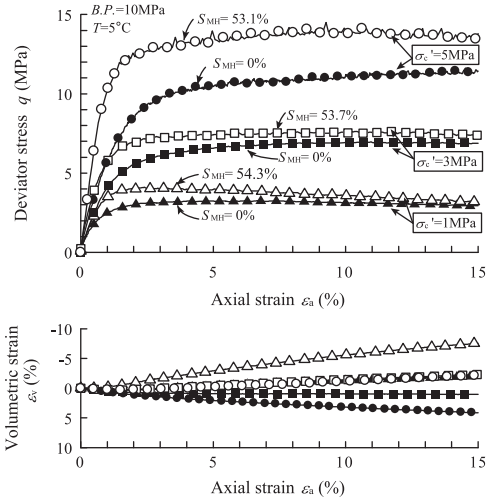

Fig. 8. Effect of effective confining pressure on the deviator stress, axial strain and volumetric strain relations for MH-bearing sand.

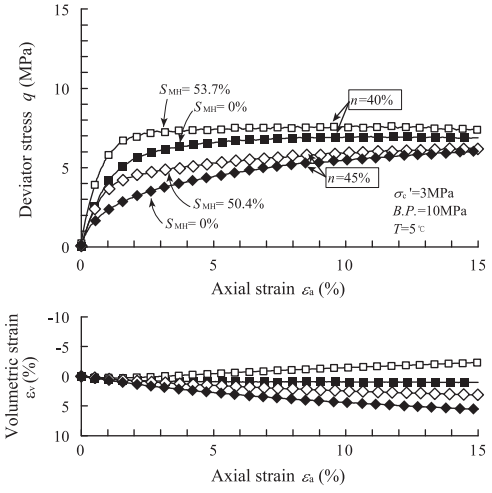

Fig. 9. Effect of relative density on the deviator stress, axial strain and volumetric strain relations for MH-bearing sand.

with the results for pure sand. For an effective confining pressure $\sigma_c'=1$ MPa, the deviator stress–axial strain behavior showed a strain softening tendency after peak, while the volumetric strain was compressive at first changing to dilative. This tendency changed with increasing effective confining pressure, i.e., the response changed gradually to a strain hardening and compressive tendency. When $\sigma_c'=5$ MPa, a clear peak was not observed and the volumetric strain became compressive.

To examine the effect of the density of the host sand, MH was generated not only in the specimen with porosity $n=40\%$ but also in the specimen with $n=45\%$. These specimens were subjected to effective confining pressure $\sigma_c'=3$ MPa and then sheared, the results of which are shown in Fig. 9. Comparing the response of the two specimens, the initial stiffness and peak strength of the specimen with $n=40\%$ appears to be higher.

Fig. 10 considers the effect of back pressure on the shear behavior by shearing specimens with similar effective confining pressure, temperature and MH saturation but different back pressure. From the figure, it is seen that the initial stiffness increases markedly while the peak strength remains higher when the back pressure was doubled.

The results of tests to examine the effect of temperature on the shear response are shown in Fig. 11. Although the temperatures considered were not much different at 1 °C and 10 °C, large differences in response can be seen with higher stiffness and higher peak strength observed for the specimen at lower temperature. By measuring the P wave velocity and S-wave velocity of artificially produced MH at temperatures of −20 to +20 °C and confining pressures of 20–100 MPa, Helgerud et al. (2009) showed that MH has temperature and back pressure dependency. They could not however distinguish between the effect of ice and methane hydrate at temperatures less than zero degrees. Since deep seabed temperatures would be above zero, tests

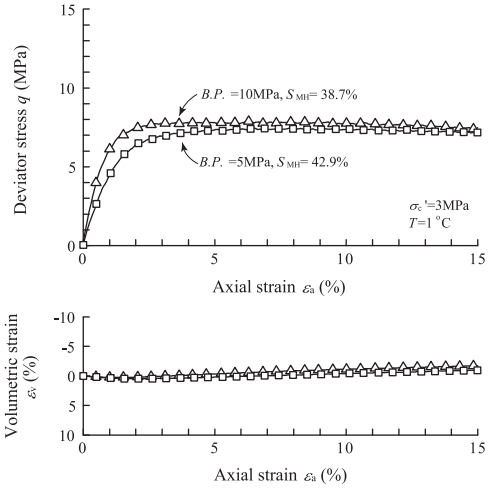

Fig. 10. Effect of pore water pressure on the deviator stress, axial strain and volumetric strain relations for MH-bearing sand.

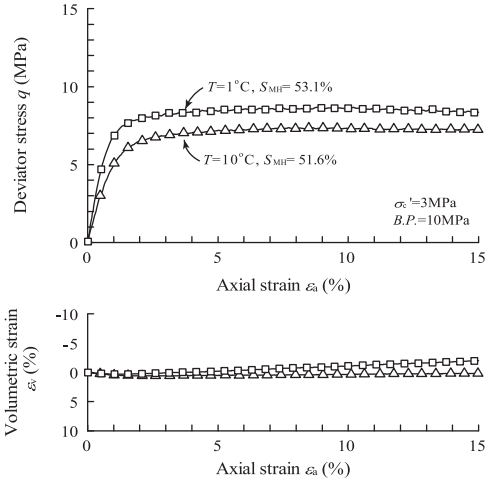

Fig. 11. Effect of temperature on the deviator stress, axial strain and volumetric strain relations for MH-bearing sand.

were performed at above zero temperatures and confirmed the temperature and pressure dependency even for these conditions.

3.3. Cementation of MH-bearing sediment

The relation between maximum deviator stress of the MH-bearing sand and MH saturation obtained from triaxial compression tests considering all experimental conditions listed in Table 1 are plotted in Fig. 12(a)–(c). Porosity and effective confining pressure are major factors affecting the shear behavior of sand. Fig. 12 presents the maximum deviator stress plotted against MH saturation for MH bearing sand with various porosities and confining pressures. Fig. 12(a), (b) and (c) show the results for effective confining stresses, $\sigma'_c = 5$ MPa, 3 MPa and 1 MPa, respectively. Furthermore, similar testing results from Miyazaki et al. (2010, 2011) are also plotted on Fig. 12(b) and (c). Although the effect of temperature and back pressure has been discussed above, their influence is relatively small when compared to that of confining pressure. It is observed from the figures that the maximum deviator stress increases with increase in MH saturation as well as with increase in confining pressure. When the three density states are compared, the increase in strength due to MH appears to be more significant for dense specimens.

Generally, it is known that the shear behavior of sands is dependent on effective stress with stress–strain curves changing from strain softening to strain hardening with increasing effective confining pressure. Moreover, loose sands have a higher tendency for strain softening behavior compared to dense. It is therefore difficult to isolate the effects of the MH cementation. Figs. 13–15 show the deviator stress differences relative to the host sand for different MH saturation, effective confining stress and relative density. The stress differences for different MH saturations at the same confining pressure of 5 MPa and porosity around 40% are summarized in Fig. 13. The peak deviator stress difference as a result of MH cementation was apparent in each case at 1%–2% strain regardless of the MH saturation. The strength decreased almost linearly with strain after the peak was reached. In Fig. 14 the relations between the deviator stress difference and axial strain for constant porosity $n = 40\%$ and MH saturation $S_{MH} = 50\%$ but varying effective confining stress $\sigma'_c = 1$, 3 and 5 MPa are depicted. The stress increment increased with increasing effective confining pressure and the maximum deviator stress difference again occurred in the vicinity of 1%–2% axial strain regardless of effective confining pressure. It should be noted that there is a frictional contribution to the strength increase rather than purely being due cementation.

To examine the influence of soil density the relation for the deviator stress differences for porosities of $n = 40\%$ (dense) and 45% (loose) are shown in Fig. 15 for a constant effective confining stress $\sigma'_c = 3$ MPa and low and high MH saturations. In this case the major influence

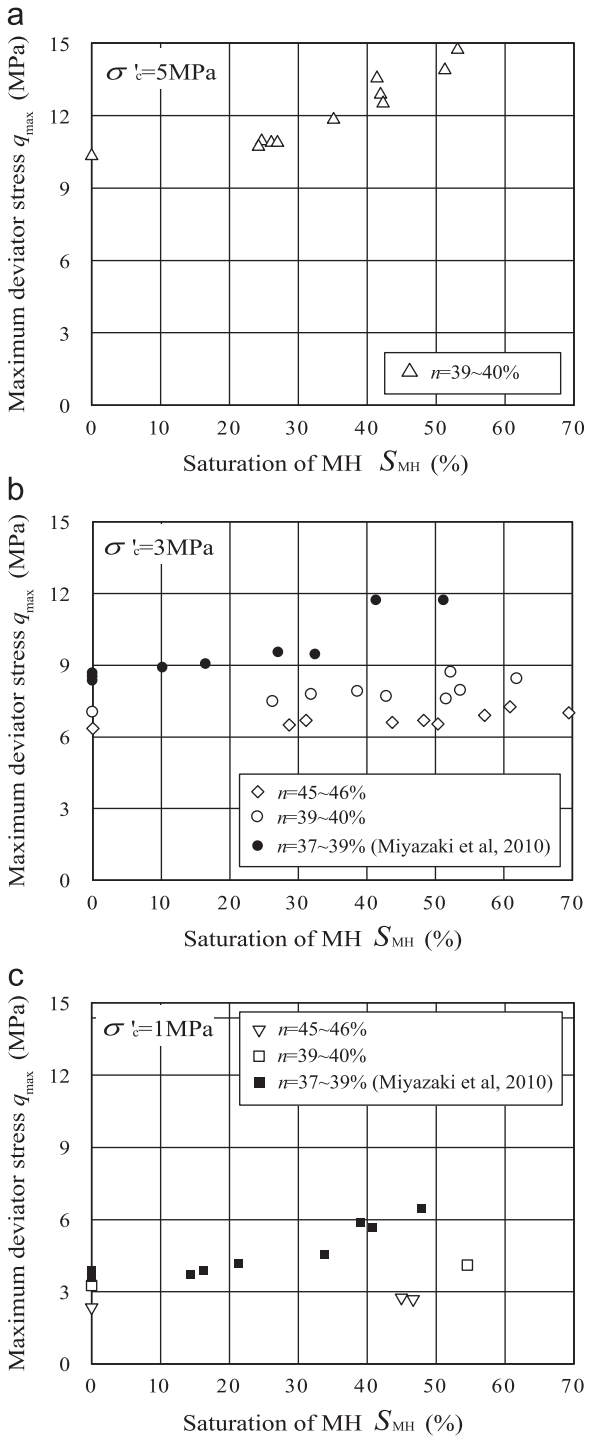

Fig. 12. Variation of maximum deviator stress with MH saturation for MH-bearing sand. (a) Confining pressure $\sigma'_c = 5$ MPa, (b) confining pressure $\sigma'_c = 3$ MPa. (c) Confining pressure $\sigma'_c = 1$ MPa.

was the MH saturation although there was a more rapid decay of strength for the loose specimens. The maximum deviator stress difference occurs at an axial strain of 1%–2% regardless of the porosity. It can also be seen that the decrease in the deviator stress difference after the peak is as marked for loose sand as it is for dense.

The strain level at which the peak increment in strength occurred due to MH cementation was 1%–2% regardless

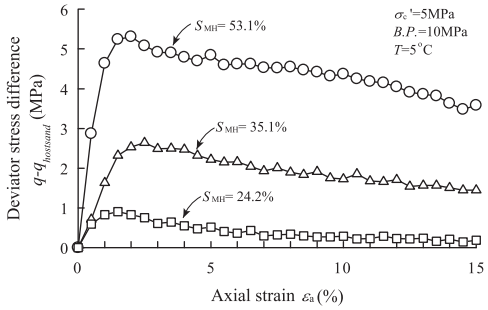

Fig. 13. Influence of MH saturation ratios on deviator stress difference versus axial strain.

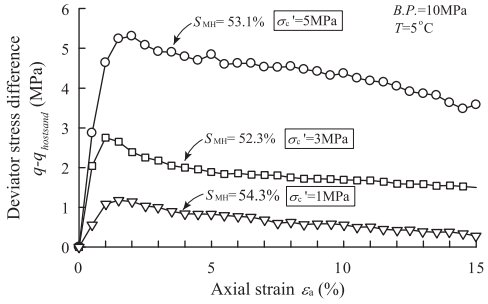

Fig. 14. Influence of confining pressure on deviator stress difference versus axial strain.

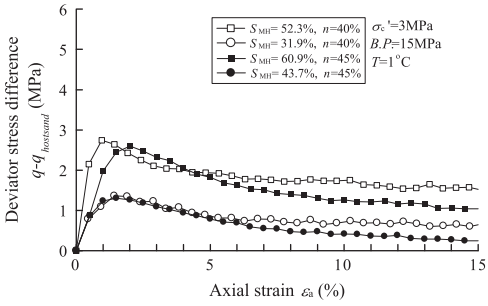

Fig. 15. Influence of sand density on deviator stress difference versus axial strain.

of the effective confining pressure, porosity and MH saturation. For the MH-bearing sand the behavior changes from compressive to dilative between 1% and 2% axial strain. Thus, it is clear that the MH cementation effect is at a maximum when the soil particles begin to roll over each other.

The relation between the deviator stress difference at an axial strain of 1.5% and MH saturation is shown in Fig. 16. Regression lines for each effective confining pressure are drawn on the figure. It is observed that the strength increase due to MH cementation increases exponentially with MH saturation. The regression lines also show that the deviator stress difference increases with increasing effective confining pressure.

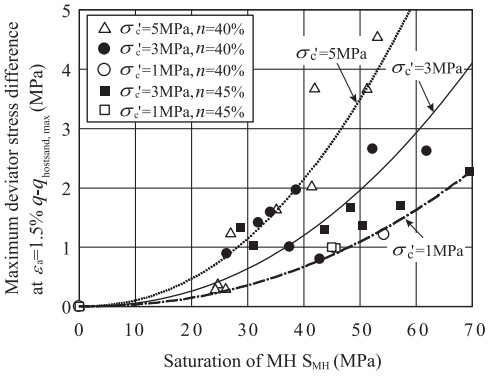

Fig. 16. Maximum deviator stress difference versus MH saturation.

In order to evaluate the influence of MH cementation on the critical state of the soil, the relation between the void ratio and mean effective principal stress during shearing is shown in Fig. 17 for all the experiments listed in Table 1. Test results for similar MH saturation levels are grouped together in Fig. 17(a)–(f). The critical state line for Toyoura sand is shown for comparison purposes in all figures. Here, it was assumed that the critical state line for a given MH saturation level is parallel to that for the Toyoura host sand. Regression lines for critical states of MH-bearing sand were drawn on each figure. These critical states lines are summarized in Fig. 17(g). It can be seen that the critical state line migrates to the right with increasing MH saturation, as the mean principal effective stress for a given void ratio increases, although there is some scatter in the data due to small variations in MH saturation. It would appear that yielding of the soil occurred at a higher mean principal stress due to MH cementation and that this cementation was not removed even under residual strength conditions.

3.4. Observation of MH-bearing sediments by Scanning Electron Microscope

The production of MH inside a cemented specimen was confirmed by removing an MH-bearing specimen before water was passed through and taking images using the scanning electron microscope (henceforth SEM) at the AIST Sapporo Laboratory (Suzuki et al., 2006a). In this machine, the test device was cooled down to −180 °C using liquefied nitrogen and the sublimation of MH or ice was controlled, making observation possible. The side for observation was not affected by frost and the specimen was cracked open inside the device. Three images corresponding to MH saturation ratios of 0%, 30% and 50% are shown in Photo 1(a)–(c), respectively. Images were magnified 100 times. All the white parts shown in Photo 1(a) are soil particles, while the grey parts in Photo 1(b) and (c) that adhered to the soil particles are MH or ice. It is clear from the images that MH clings to the soil particles and covers their surfaces. Moreover, the MH was uniformly distributed, confirming its uniformity within the specimen.

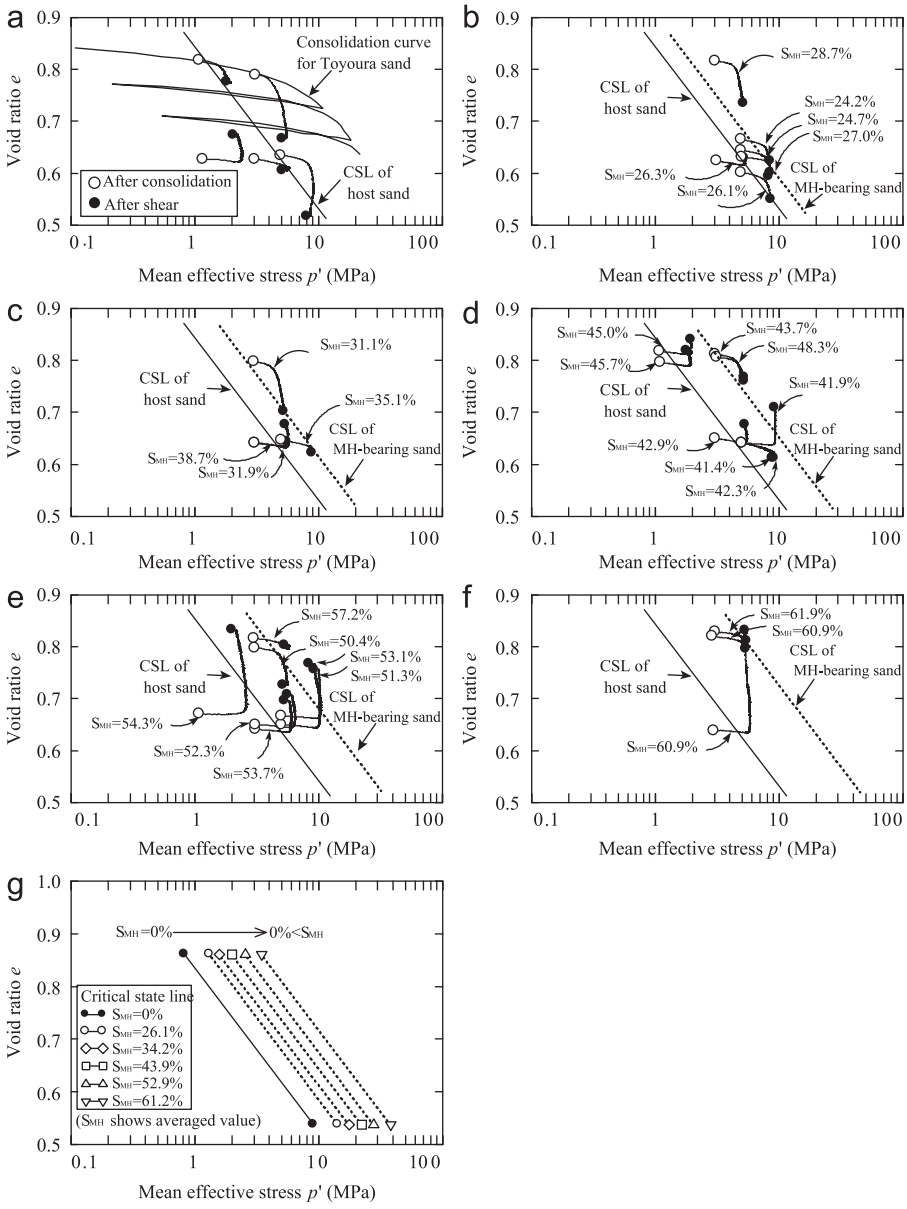

Fig. 17. Relationship between void ratio and mean effective stress during compression shear tests. (a) S_{MH}=0%, (b) S_{MH}=20%–30%, (c) S_{MH}=30%–40%, (d) S_{MH}=40%–50%, (e) S_{MH}=50%–60%, (f) S_{MH}=60%∼ and (g) critical state lines for MH-bearing sand.

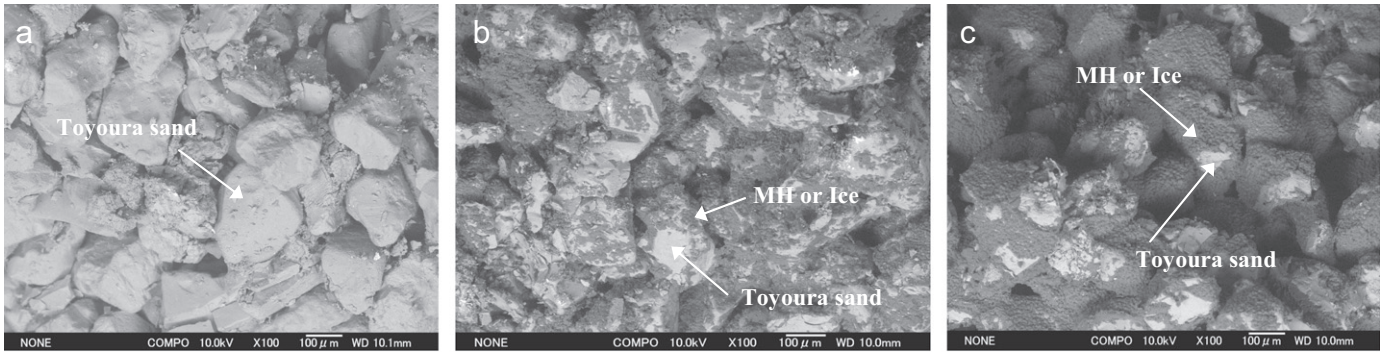

Photo 1. SEM images of specimen prepared (magnified 100 times): (a) S_{MH}=0%; (b) S_{MH}=30%; (c) S_{MH}=50%. (a) S_{MH}=0%. (b) S_{MH}=30%. (c) S_{MH}=50%.

Table 2
Test conditions and experimental results for MH dissociation tests.

Testing condition						Testing result		Remarks
Production methods		Consolidation condition	σ'_c (MPa	*P.P.* (MPa	*T* (°C)	*n* (%)	S_{MH} (%)	
Thermal recovery	5→20 (°C)	Iso	5	10	5	39.6	46.0	Consolidation→production
						39.1	47.3	Loaded to deviator stress $q=8$ (MPa) after consolidation→production
						39.1	48.0	Loaded to deviator stress $q=12$ (MPa) after consolidation→production
Depressurization	10→3.5 (MPa) (0.5 MPa/min)	Iso	5	10	5	39.3	31.5	Consolidation→production after production→water pressure recover
						39.0	43.2	Loaded to deviator stress $q=8$ (MPa) after consolidation→production After production→Water pressure recover
						39.3	38.2	Loaded to deviator stress $q=12$ (MPa) after consolidation→production After production→water pressure recover

4. MH dissociation tests

4.1. Testing condition and stress path of dissociation tests

After consolidation at an effective stress equivalent to in-situ conditions, MH dissociation was performed by either increasing the temperature or decreasing the pressure. The experimental conditions and the corresponding experimental results are summarized in Table 2. Fig. 18 shows the stress paths followed for three different cases. In Case 1 there was no initial shear stress and the temperature was increased to simulate thermal recovery or the mean principal effective stress was increased from a to a′ simulate the depressurization method. In the case of depressurization, the back pressure was allowed to increase again after dissociation to represent post-production equilibrium conditions being restored. In Case 2 an initial shear stress was applied before using thermal recovery or depressurization. Following this the temperature was allowed to increase at b or the back pressure was decreased from b to b′, and from b′ back to b after the dissociation of all the MH. Finally in Case 3 the stress path was taken into the metastable zone between the failure envelopes for pure sand and MH-bearing sand. The purpose of this test was to study the effect of dissociation and consequent loss of particle bonding in the zone where failure could occur for unbonded sand.

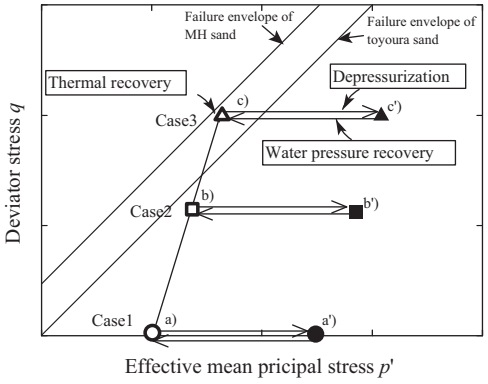

Fig. 18. Stress paths for Thermal recovery, depressurization and water pressure recovery.

4.2. Thermal recovery method

The temperature was increased to cause dissociation by circulating heated oil through a double walled annulus surrounding the inner cell. Fig. 19 shows the deviator stress, axial strain and volumetric strain relations for isotropically consolidated $n=40\%$ specimens ($Dr=90\%$)

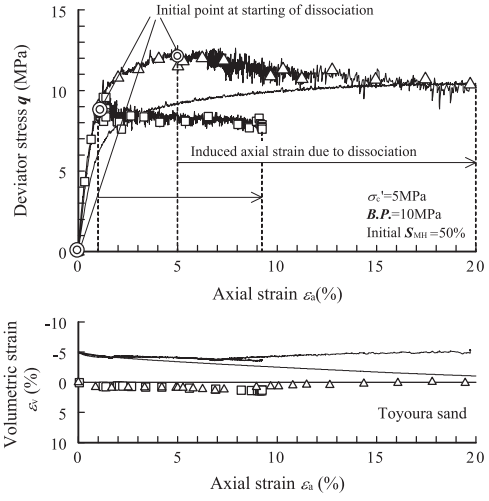

Fig. 19. Stress strain behavior during MH dissociation using thermal recovery.

for Case 1, Case 2 and Case 3 subjected to an initial effective confining pressure $\sigma_c'=5$ MPa. Axial load was controlled constant after initial shear stress applied. From the figure, it is observed for Case1 that no deformation was occurring during the dissociation of MH. Next, in Case 2, the axial strain increased to $\varepsilon_a=9\%$, however, failure conditions were not reached. Finally, in Case 3, it was observed that the sediment failed due to dissociation of MH. That is, the sediment will collapse when the methane hydrate dissociates in the state between the failures envelopes for pure sand and MH-bearing sand. Besides, deviator stress decreased during thermal recovery in Case 2 and Case 3, because axial load was not controlled completely constant due to deformation occurred very quickly.

Fig. 20 shows the variation of temperature, MH saturation, and volumetric and axial strains with elapsed time. For stress state (a) there was only a small change in axial strain related to the small volumetric compression. For stress state (b) there was a marked increase in axial strain reaching about 10% as the MH dissociated. Total collapse did not occur as the soil was still below the failure envelope. In the case of stress state (c) the strain initially increased until the start of MH dissociation when a rapid collapse occurred as the failure envelope moved towards that for the uncemented sand.

The thermal method required the input of heating energy. During this process deformation of the soil occurred under high initial shear stresses indicating that should this method be used for methane production high levels of deformation could occur.

4.3. Depressurization method

Fig. 21 shows the variation of back pressure, MH saturation, volumetric and axial strains during the depressurization and re-pressurization stages. In each case there was an initial compressive volumetric strain because of the increase in effective stress. Further volumetric strain occurred as the MH dissipated and bonds dissolved. Dissociation occurred when the back pressure dropped to 4.3 MPa. Dissociation continued for approximately 2 to 3 h from initiation, with axial strains still increasing up to 3 h after the start of the test. After 5 h the back pressure was ramped back up to 10 MPa over one hour to represent a restoration of post-dissociation equilibrium conditions being restored in-situ. In Cases 1 and 2 there was an elastic recovery of axial and volumetric strains due to a decrease in effective stress. However in Case 3 collapses occurred as the now non-bonded soil moved outside the failure envelope.

Fig. 22 shows the stress ratio η (q/p'), axial strain and volumetric strain relations during the tests. It can be seen that the axial strain increased dramatically when the stress strain curve reached the strength of pure sand as the water pressure recovered.

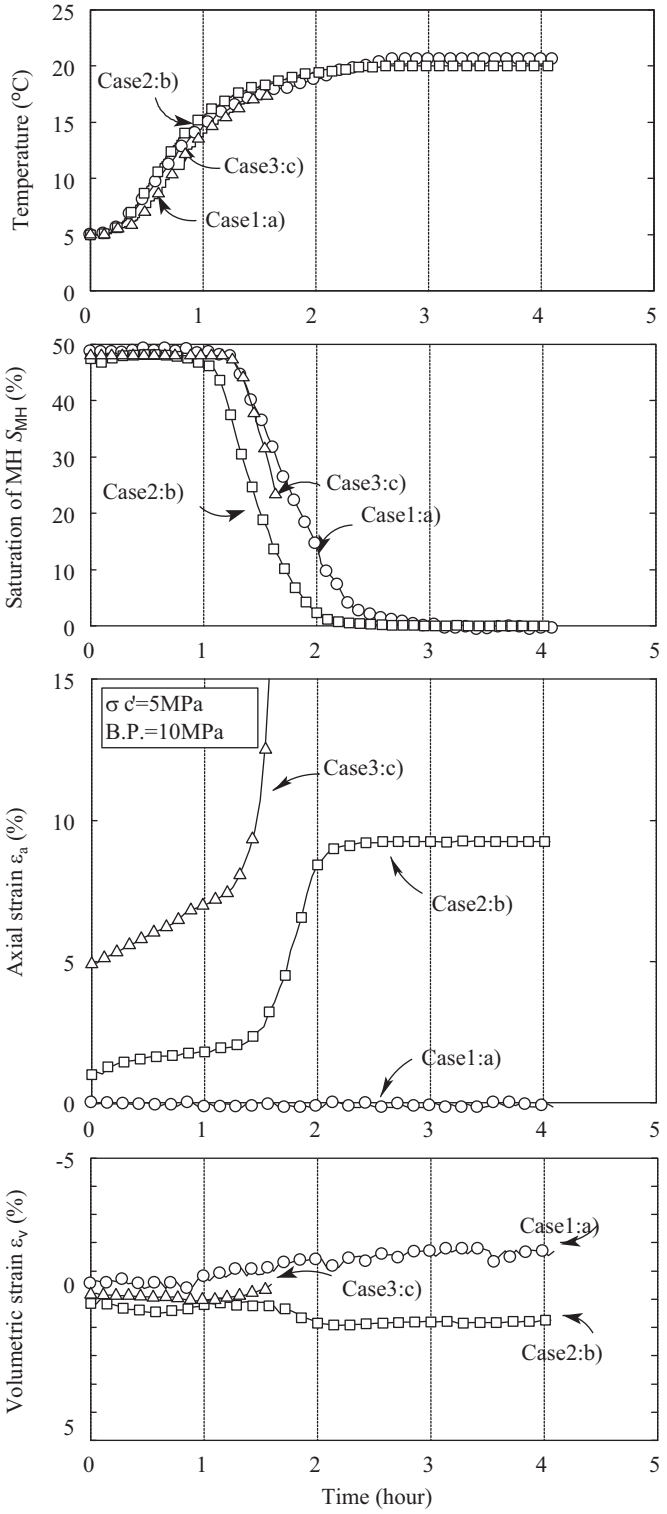

Fig. 20. Variation of temperature, MH saturation, and volumetric and axial strains with elapsed time.

In contrast to the thermal method no deformations were observed despite the increase in effective stresses. After dissociation during back pressure recovery large deformations may occur in the metastable zone. In the Nankai trough the geology consists of turbidite alternating layers

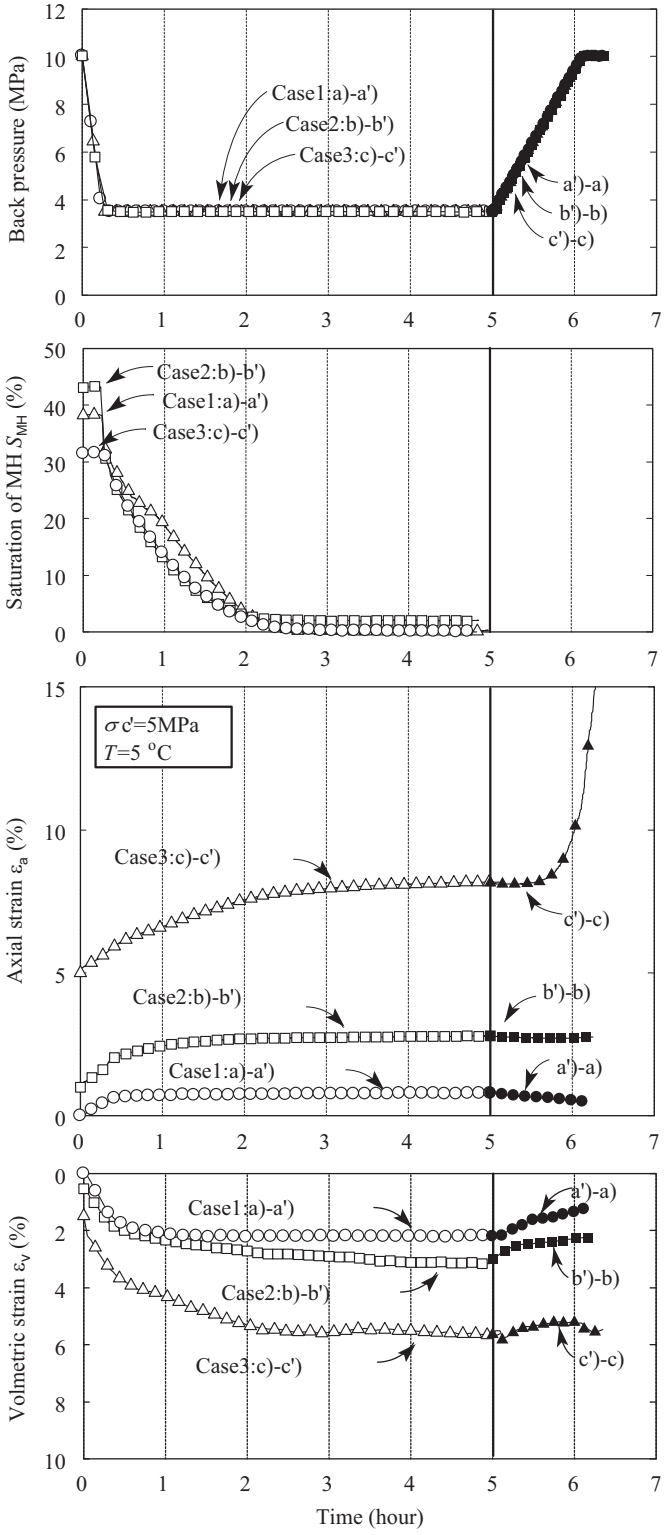

Fig. 21. The variation of pore pressure, MH saturation, volumetric and axial strains during de-pressurization and re-pressurization .

of sands and clays. Where the sands containing the methane hydrate are sandwiched between impermeable clay layers the depressurization method would be most effective.

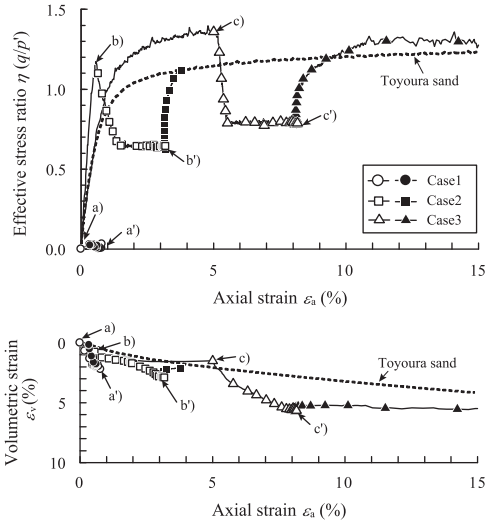

Fig. 22. Stress strain behavior during MH dissociation using depressurization and water pressure recovery.

4.4. Observations of MH dissociation

In order to observe the disappearance of MH cementation, images were taken of the test specimen, during MH dissociation by heating, using SEM continuous images, magnified 200 times, as shown in Photo 2(a)–(d). Photo 2(a) shows the specimen with an MH saturation of 50% where initially, the soil particles are covered by MH. Focusing on regions between soil particles, the arrows indicate where MH exists adjacent to the hardened particles. Photo 2(b) and (c) were taken during the MH dissociation process. Comparing these figures, it can be observed that the MH on the surface of the soil particles gradually disappeared while the hydrates, which seem to connect the particles as indicated by the arrows, appear to remain up to the last minute.

5. Conclusions

In the Nankai trough the geology consists of turbidite alternating layers of sands and clays. Where the sands containing the methane hydrate are sandwiched between impermeable clay layers the depressurization method would be most effective. The Japan's MH production program is going to apply the depressurization method to the production of MH. Additionally, heating method will be applied to promote the production more effectively. The present research was done in order to understand the fundamental mechanical and dissociation properties on MH bearing sands.

The following conclusions were drawn:

1) Artificial samples containing methane hydrate were successful produced by controlling stress and temperature conditions.
2) The strength of MH sand increased with MH saturation for the test on MH-bearing sand with $S_{MH} < 30\%$.

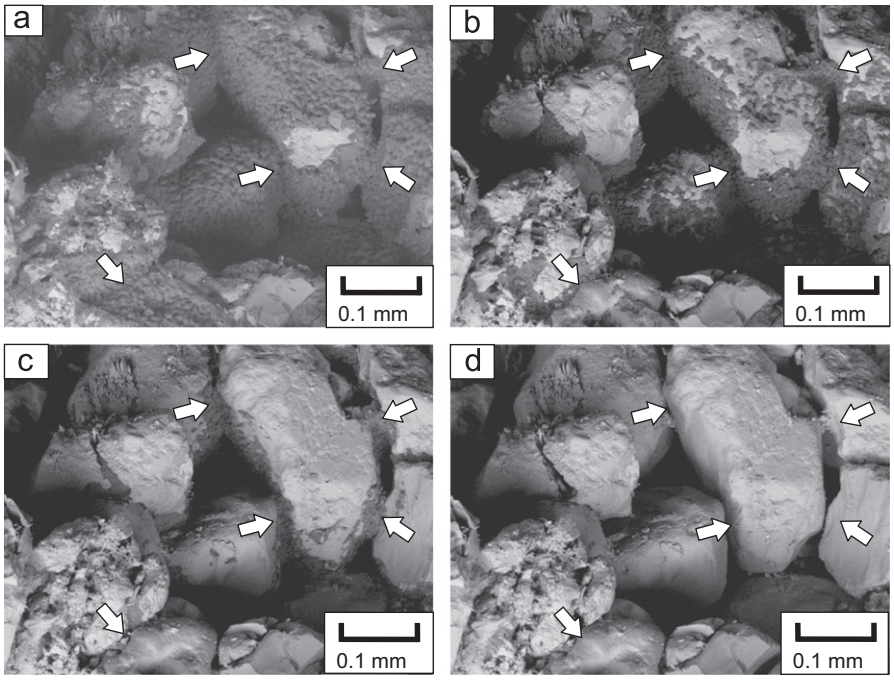

Photo 2. SEM images magnified 200 times of specimens (a) MH saturation 50%; (b) & (c) during MH dissociation; and (d) MH saturation of 0%.

On the other hand, the higher strength on specimens with $30\% < S_{MH}$ is postulated to be due to the particle bonding and the contribution of MH flakes which were peeled off from sand particle surfaces and were buried within the pores of the sand during shearing.

3) The peak strength increased with increasing effective confining pressure indicating that there is a frictional contribution to the strength increase rather than purely being due to cementation.
4) The maximum deviator stress difference occurred in the vicinity of 1%–2% axial strain regardless of effective confining pressure. Thereafter the strength decreased linearly with increasing axial strain.
5) The strength of MH sand increased with increasing back pressure and decreasing temperature.
6) Dissociation by heating caused large axial strains for samples with an initial shear stress and total collapse for samples consolidated in the metastable zone.
7) In the case of dissociation by de-pressurization, axial strains were generated by increasing effective stress until a stable equilibrium was reached. However re-pressurization led to the collapse of Case 3 in the metastable zone.

Acknowledgments

A part of the present work was done as the activity of Research Consortium for Methane Hydrate Resources in Japan. The authors would like to express their sincere thanks to their supports.

References

Fujii, T., et al, 2008. Resource assessment of methane hydrate in the Eastern Nankai Trough, Japan. In: Proceedings of the 2008 Offshore Technology Conference, OTC19310.

Fujii, T., Saeki, T., Kobayashi, T., Inamori, T., Hayashi, M., Takano, O., Takayama, T., Kawasaki, T., Nagakubo, S., Nakamizu, M., Yokoi, K., 2009. Resource assessment of methane hydrate by applying a probabilistic, approach in the Eastern Nankai Trough. Journal of Geography 118 (5), 814–834 (in Japanese).

Helgerud, M.B., Waite, W.F., Kirby, S.H., Nur, A., 2009. Elastic wave speeds and moduli in polycrystalline ice Ih, sI methane hydrate, and sII methane–ethane hydrate. Journal of Geophysical Research 114, B02212.

Hyodo, M., Hyde, A.F.L., Nakata, Y., Yoshimoto, N., Fukunaga, M., Kubo, K., Nanjo, T., Matsuo, T., Nakamura, K., 2002. Triaxial compressive strength of methane hydrate. In: Proceedings of 12th International Offshore and Polar Engineering Conference, pp. 422–428.

Hyodo, M., Nakata, Y., Yoshimoto, N., Ebinuma, T., 2005. Basic research on the mechanical behavior of methane hydrate-sediments mixture. Soils and Foundations 45 (1), 75–85.

Hyodo, M., Nakata, Y., Yoshimoto, N., Yoneda, J., 2007. Mechanical behavior of methane hydrate-supported sand. In: Proceedings of the International Symposium on Geotechnical Engineering, Ground Improvement and Geosynthethics for Human security and Environmental Preservation, pp. 195–208.

Hyodo, M., Nakata, Y., Yoshimoto, N., Yoneda, J., 2008. Shear strength of methane hydrate bearing sand and its deformation during dissociation of methane hydrate. In: Proceedings of the 4th International Symposium on Deformation Characteristics of Geomaterials, pp. 549–556.

Kvenvolden, K.A., Ginsburg, G.D., Soloviev, V.A., 1993. Worldwide distribution of subaquatic gas hydrates. Geo-Marine Letters 13, 32–40.

Lee, J.Y., Carlos Santamarina, J., Ruppel., C., 2010. Volume change associated with formation and dissociation of hydrate in sediment. Geochemistry Geophysics Geosystems 11, Q03007.

MH21 Research Consortium, 2001 Research Consortium for Methane Hydrate Resources in Japan. 〈http://www.mh21japan.gr.jp/〉.

Miyazaki, K., Masui, A., Sakamoto, Y., Haneda, H., Ogata, Y., Aoki, K., Yamaguchi, T., Okubo, T., 2007. Effect of strain rate on the preparation of triaxial compression test specimen of deposits containing methane hydrate. Journal of MMIJ 123 (11), 537–544 (in Japanese).

Miyazaki, K., Yamaguchi, T., Sakamoto, Y., Tenma, N., Ogata, Y., Aoki, K., 2010. Effect of confining pressure on mechanical properties of sediment containing synthetic methane hydrate. Journal of MMIJ 126 (7), 408–417 (in Japanese).

Miyazaki, K., Masui, A., Sakamoto, Y., Aoki, K., Tenma, N., Yamaguchi, T., 2011. Triaxial compressive properties of artificial methane-hydrate-bearing sediment. Journal of Geophysical Research 116, B06102. http://dx.doi.org/10.1029/2010JB008049.

Nagakubo, S., 2009. Methane hydrate as a domestic energy resource: Japan's methane hydrate R&D program. Journal of Geography 118 (5), 758–775 (in Japanese).

Oda, K., Nakata, Y., Hyodo, M., Murata, K., Haba, S., Yoneda, O., 1998. Direct shear behavior of sand with hardening force between particles. In: Proceedings of the 33rd Japan National Conference on Geotechnical Engineering, pp. 663–664 (in Japanese).

Sakamoto, Y., Shimokawara, M., Oga, H., Miyazaki, S., Komai, T., Aoki, K., Yamaguchi, T., 2008. Laboratory tests on the consolidation behavior and seepage characteristics of methane hydrate during dissociation by depressurization method. Journal of MMIJ 124 (8), 498–507 (in Japanese).

Sloan, E.D., 1998. Clathrate Hydrate of Natural Gases, 2nd ed. Marcel Dekker, Inc., New York 705p.

Suzuki, K., Nagao, J., Narita, H.,2006a. Observation of gas hydrate production in sediment deposits using scanning electron microscope. In: Proceedings of the Annual Conference of the Japan Geoscience Union, G228-006 (in Japanese).

Suzuki, K., Hyodo, M., Nakata, Y., Yoshimoto, N., 2006b. Consolidation characteristics of methane hydrate-bearing deposits in Nankai Trough. Shigentosozai (A/B), 167–168 (in Japanese).

Suzuki, K., Ebinuma, T., Narita, H., 2009. Features of methane hydrate-bearing sandy-sediments of the forearc basin along the Nankai trough: effect on methane hydrate-accumulating mechanism in turbidite. Journal of Geography 118 (5), 899–912 (in Japanese).

Yamamoto, K., 2009. Production Techniques for methane hydrate resources and field test programs. Journal of Geography 118 (5), 913–934 (in Japanese).

Yasufuku, N., Murata, H., Hyodo, M., 1991. Yield characteristics of anisotropically consolidated sand under low and high stresses. Soils and Foundations 31 (1), 95–109.

Yoneda, J., Hyodo, M., Nakata, Y., Yoshimoto, N., Kokura, Y., Tsuda, N., Ebinuma, T., 2007a. Mechanical characteristics of MH-bearing sand during dissociation by depressurization method. In: Proceedings of the 42nd Japan National Conference on Geotechnical Engineering, pp. 321–322 (in Japanese).

Yoneda, J., Hyodo, M., Nakata, Y., Yoshimoto, N., Kokura, Y., Tsuda, N., Ebinuma, T., 2007b. Mechanical property of gas hydrate sediment at deep seabed on triaxial compression test. Ground Engineering 25 (1), 113–122 (in Japanese).

Yoneda, J., Hyodo, M., Nakata, Y., Yoshimoto., 2010. Triaxial shear characteristics of methane hydrate-bearing sediment in the deep seabed. Journal of Geotechnical Engineering (III), 66 (4), 742–756 (in Japanese).

Yun, T.S., Santamarina, J.C., Ruppel, C., 2007. Mechanical properties of sand, silt, and clay containing tetrahydrofuran hydrate. Journal of Geophysical Research 112, B04106.

Waite, W.F., Santamarina, J.C., Cortes, D.D., Dugan, B., Espinoza, D.N., Germaine, J., Jang, J., Jung, J.W., Kneafsey, T.J., Shin, H., Soga, K., Winters, W.J., Yun, T.-S., 2009. Physical properties of hydrate-bearing sediments. Reviews of Geophysics 47, RG4003.